Highly Efficient Phosphate Scavenger Based on Well-Dispersed $La(OH)_3$ Nanorods in Polyacrylonitrile Nanofibers for Nutrient-Starvation Antibacteria

Jiaojie He,[†,∥] Wei Wang,[*,†,∥] Fenglian Sun,[†] Wenxin Shi,[†] Dianpeng Qi,[‡] Ke Wang,[†] Ruisha Shi,[†] Fuyi Cui,[*,†] Ce Wang,[§] and Xiaodong Chen[‡]

[†]State Key Laboratory of Urban Water Resource and Environment (SKLUWRE), School of Municipal and Environmental Engineering, Harbin Institute of Technology, Harbin 150090, P.R. China, [‡]School of Materials Science and Engineering, Nanyang Technological University, 639798, Singapore, and [§]Alan G. Macdiarmid Institute, Jilin University, Changchun 130012, China. [∥]J.H. and W.W. are cofirst authors.

ABSTRACT $La(OH)_3$ nanorods immobilized in polyacrylonitrile (PAN) nanofibers (PLNFs) were fabricated for the first time by electrospinning and a subsequent *in situ* surfactant-free precipitation method and then applied as a highly efficient phosphate scavenger to realize nutrient-starvation antibacteria for drinking water security. The immobilization by PAN nanofibers effectively facilitated the *in situ* formation of the aeolotropic and well-dispersed $La(OH)_3$ nanostructures and, thus, rendered higher phosphate removal efficiency due to more exposed active sites for binding phosphate. The maximum phosphate capture capacity of $La(OH)_3$ nanorods in PAN nanofibers was around 8 times that of the $La(OH)_3$ nanocrystal fabricated by precipitation without PAN protection. Moreover, remarkably fast adsorption kinetics and high removal rate were observed toward low concentration phosphate due to the high activity of our materials, which can result in a stringent phosphate-deficient condition to kill microorganisms in water effectively. The present material is also capable of preventing sanitized water from recontamination by bacteria and keeping water biologically stable for drinking. Impressively, stabilized by PAN nanofibers, the $La(OH)_3$ nanorods can be easily separated out after reactions and avoid leaking into water. The present development has great potential as a promising antimicrobial solution for practical drinking water security and treatment with a negligible environmental footprint.

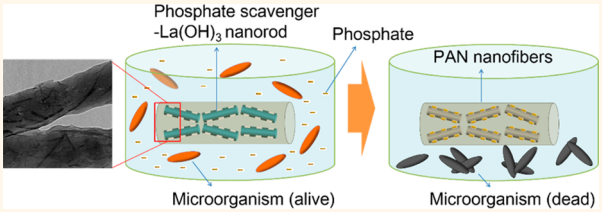

KEYWORDS: electrospinning · phosphate removal · drinking water security · antibacteria · $La(OH)_3$

Microbiological contamination in drinking water constitutes one of the greatest global challenges facing both environmental sustainability and public healthcare today.[1,2] Rapid bacterial regrowth occurs frequently even in sanitized water, particularly in tropical and subtropical countries where high humidity and temperatures complicate maintenance of clean water storage units, threatening human health. A general method to limit microbial growth is the addition of excess disinfectants (*e.g.*, chlorine, chlorine dioxide, or ozone) into drinking water, yet the toxicity of disinfection byproducts leads to a quest for alternative solutions.[3] Recently, there has been a huge advancement in the development of new types of antibacterial materials, such as silver particles, poisonous oxides, antibiotics, photosensitizers, hydrogels, and antimicrobial peptides.[4−8] Most antimicrobial materials react with living cells by releasing toxic substances,[9,10] which would result in health risks in drinking water; other antibacterial agents are confined to physical contact with microorganisms,[4,11,12] which is not promising for large-scale water supplies.

Phosphorus, an essential element for the growth of all organisms, serves as a main building block for energy carriers, nucleic acids, and proteins.[3] An excessive intake of phosphorus in water bodies spurs abnormal growth of algae and aquatic plants.[13] It is widely accepted that phosphate is the only form of phosphorus that can be directly assimilated by microorganisms, algae, and other planktons.[14] Consequently, efficient

* Address correspondence to wangweirs@hit.edu.cn, cuifuyi@hit.edu.cn.

Received for review July 9, 2015 and accepted August 12, 2015.

Published online August 20, 2015
10.1021/acsnano.5b04236

phosphate removal in water is expected to be a green strategy to prevent the growth of microorganisms, which would bypass toxic substances released from antibacterial agents. Although measures have been developed to remove phosphate from water, such as chemical precipitation, biological processes, adsorption, ion exchange, and so on,[13−17] most of which cannot provide satisfactory low levels of phosphate after treatment to suppress microbial growth. Lanthanum (La) species, particularly nanostructures, known to bind very strongly to phosphate (solubility product of lanthanum phosphate pK = 26.16), have been recently employed to adsorb excess phosphate in the human body (Fosrenol) and in water and exhibited superior adsorption capacity and high removal rate,[13,18−26] thus holding great potential toward reducing algae and bacteria overgrowth.[27,28] However, (i) conventional lanthanum-containing nanostructures usually tend to agglomerate to minimize their surface energy, causing the inner regions of the resulting aggregates to not be effectively utilized and thus suppressing the removal efficiency toward low concentration phosphate.[29] (ii) Most seriously, the leakage of La into water, which probably renders biological incompatibilities like taking a toll on animal and human's central nervous system,[30] poses a huge challenge for those La-containing phosphate scavengers hitherto developed in practical application for drinking water security.[24,26,28] The leakage problem is associated with both the complicated liquid−solid separation of those traditional powdered agents and the structural instability of them in water solution. Although loading La_2O_3 nanoparticles into filter membranes was effective to reduce leaking,[3] the water flux declined by 95% in a short time due to the severe membrane fouling and thus hindered the practical application. Therefore, it is earnestly desired to design a safe and highly efficient phosphate scavenger for nutrient-starvation antibacteria in drinking water.

Electrospinning is a remarkably facile and versatile method to fabricate nanofibers and submicrofibers with ultrahigh aspect ratio for a broad range of applications (catalysis, adsorption, sensing, *etc.*). Particularly powerful for this technique, nanosized functional components with homogeneous dispersion can be conveniently incorporated and stabilized in fiber matrixes.[31−38] Given the excellent spinnability, environmentally benign nature, hydrostability, and hydrophilicity of polyacrylonitrile (PAN),[39] well-dispersed $La(OH)_3$ nanorods impregnated in PAN nanofibers (PLNFs) were produced for the first time by electrospinning combined with a subsequent *in situ* precipitation process at room temperature for phosphate-starvation antibacteria. The superlong PAN nanofibers served not only as a facilitator for the *in situ* formation of the well-dispersed $La(OH)_3$ nanorods but also as a stabilizer to avoid lanthanum leakage during application. By this hierarchical nanostructure, the maximum phosphate capture capacity toward 80 mg P/L solution was increased to 172.2 mg P/g (lanthanum), around 8 times that of conventional $La(OH)_3$ nanocrystal fabricated by precipitation without PAN protection. Moreover, a fast kinetics and high-removal efficiency were observed for the adsorption of low concentration phosphate (2 mg/L) owning to the high activity of our materials, which can result in a stringent phosphate-deficient condition to kill microorganisms in water effectively. PLNFs are also capable of preventing sanitized water from the recontamination by bacteria for drinking. The present materials have great application potential in securing biological stability during water production, supply, as well as storage due to their high efficiency and excellent safety.

RESULTS AND DISCUSSION

Materials Fabrication and Characterization. 1D $La(OH)_3$, with outstanding application in catalysis, optical devices, electronics, and magnetic equipment, was rationally synthesized by using hydrothermal method, solvothermal strategy, precipitation, and microwave-assisted routes in recent years.[40−44] Among these fabrication methods, the precipitation route concerning the reaction between alkali and La^{3+}-containing solution at low temperature was widely applied due to its simplicity, high efficiency, and low cost.[43,45] In general precipitation processes, organic molecular surfactants with growth-controlling and agglomeration-inhibiting functions were strictly required to direct the growth of the anisotropic 1D $La(OH)_3$.[45,46] In the present work, we developed a facile *in situ* precipitation without addition of any surfactant by the aid of electrospinning technology. First, $La(NO_3)_3$ was incorporated into PAN (a water-insoluble polymer with good hydrophilicity) nanofibers via an electrospinning process. Then the NaOH solution was used to treat the precusor composite nanofibers and *in situ* converted the $La(NO_3)_3$ inside the fibers into $La(OH)_3$ at room temperature. During the formation process above, the PAN nanofiber matrix was expected to serve as both a growth controller and an agglomeration inhibitor for forming the $La(OH)_3$ nanorods.

The digital picture of the PLNFs is shown in Figure S1 in the Supporting Information. Figure 1a and the inset provide the scanning electron microscopy (SEM) images of the PLNFs mats at different magnifications after electrospinning and a subsequent *in situ* treatment by NaOH solution for 12 h. Just as the typical electrospun products, the fibers randomly oriented, with an average diameter of around 185 nm (calculated in Figure S1). TEM characterization (Figure 1b and Figure S2) gave further insight into the morphology and structural features of the products. As shown in Figure 1b, $La(OH)_3$ was observed as dark rodlike structures in the PAN nanofiber matrix, displaying an average length of ∼59 nm (inset of Figure 1b) and an

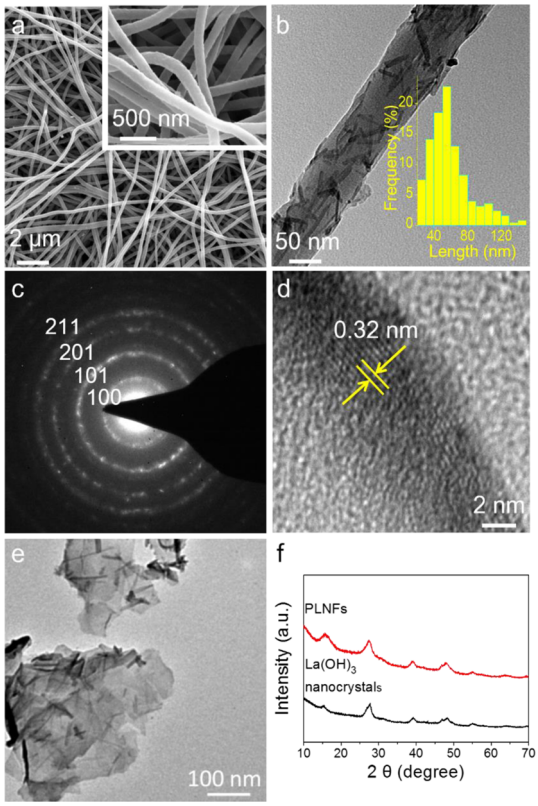

Figure 1. (a) SEM images of the PLNFs mats at different magnifications. (b) TEM image of the PLNFs (inset: length distribution of $La(OH)_3$ nanorods in the PAN matrix). (c) Selected-area electron diffraction (SAED) pattern. (d) HRTEM image of the PLNFs. (e) Morphology (TEM) of $La(OH)_3$ nanocrystal formed by conventional precipitation without PAN fibers. (f) Corresponding XRD spectra of the above two samples.

average diameter of ~6 nm. The selected-area electron diffraction (SAED) pattern of $La(OH)_3$ nanorods in Figure 1c showed the polycrystalline diffraction rings, corresponding to the (100), (101), (201), and (211) planes of hexagonal $La(OH)_3$.[45] The structure of an individual nanorod in the PLNFs was further examined by high-resolution transmission electron microscopy (HRTEM) as shown in Figure 1d, which displayed a well-defined crystallinity with a lattice spacing of 0.32 nm, ascribed to the (101) plane of hexagonal $La(OH)_3$.[47]

To better understand the role of the PAN nanofibers in the formation of the $La(OH)_3$ nanorods, a control sample of pure $La(OH)_3$ nanocrystal was fabricated by a conventional precipitation method (CPM) to compare with PLNFs shown in Figure 1e. The reaction between NaOH and $La(NO_3)_3$ solution was carried out, without addition of PAN or any organic surfactant. It was found that in the absence of PAN the pure $La(OH)_3$ nanocrystal (Figure 1e) exhibited an irregular morphology, with only a few rodlike structures appearing in the $La(OH)_3$ aggregates.[42,45] The X-ray diffraction (XRD) patterns of the two products are shown in Figure 1f. Several characteristic peaks such as the (100), (110), (101), (201), (300), (211), and (112) planes of $La(OH)_3$ were observed for both the pure $La(OH)_3$ nanocrystal and the PLNFs, which were located at $2\theta = 15.6$, 27.3, 27.9, 39.5, 48.2, 48.5, and 55.2°, respectively (JCPDS card no. 83-2034).[26] The lanthanum contents in PLNFs and pure $La(OH)_3$ nanocrystal were detected by ICP-OES to be 7.8 and 71.1 wt %, respectively.

The time-dependent growth process of the $La(OH)_3$ in the PAN nanofibers during *in situ* precipitation was also studied and is shown in Figure 2. Before treatment by NaOH, no distinct La-based crystals were observed in the PAN fibers by TEM (Figure 2a), which was similar to the prior report on inorganic salt/polymer composite nanofibers.[48] When the samples were treated by NaOH for a short time (30 min), a few dark nanodots emerged (Figure 2b) and grew in size with increasing time (1 h, Figure 2c). As the immersion time in NaOH further increased, many nanodots agglomerated (2 h, Figure 2d) along a 1D direction and subsequently formed short nanorods (6 h, Figure 2e). Finally, after being soaked in NaOH solution for more than 10 h, the *in situ* $La(OH)_3$ nanorods with a definite 1D configuration in PAN naofibers were formed (Figure 2f,g). When the treatment time was increased to 12 h, there was an insignificant change in the structure of the $La(OH)_3$ nanorods (Figure S3). Thus, on the basis of the above observation, a possible formation process for the $La(OH)_3$ nanorods was proposed and is schematically displayed in Figure 2h. $La(OH)_3$ fabricated by precipitation in alkaline condition tended to form anisotropic structures due to the intrinsical anisotropy of the hexagonal $La(OH)_3$,[49] which is confirmed by Figure 1e, and the results are reported in the literature.[43] In a conventional precipitation process, in order to produce better-structured 1D $La(OH)_3$, organic molecular surfactant micelles in the aqueous solution served as a template for assembling lanthanum cations inside and influenced the nucleation and growth process of the crystals.[45] In the present work, La^{3+} was directly incorporated into the PAN nanofibers by electrospinning. Accordingly, PAN fibers acted as a nanoreactor, which could not only provide a place for the reaction between La^{3+} and alkali solution but also impact the nucleation and growth process of the assemblies. By the growth-controlling and agglomeration-inhibiting functions of the PAN fibers, as well as the intrinsical anisotropy of the hexagonal structure $La(OH)_3$,[47] the aeolotropic structure was finally formed.

PAN nanofibers impregnated with various ratios of $La(OH)_3$ were also prepared by electrospinning and *in situ* precipitation. The initial mass ratios of PAN to $La(NO_3)_3 \cdot 6H_2O$ in the PAN/$La(NO_3)_3$ precusor nanofibers were 10:1, 6:1, and 3:1, respectively. After 12 h incubation in NaOH, the resulting PAN/$La(OH)_3$ nanofibers were characterized by TEM and then shown in Figure 3. When the initial concentration of $La(NO_3)_3$ was lower, $La(OH)_3$ had not formed a nanorod structure yet in 12 h. When the PAN/$La(NO_3)_3 \cdot 6H_2O$ ratio was

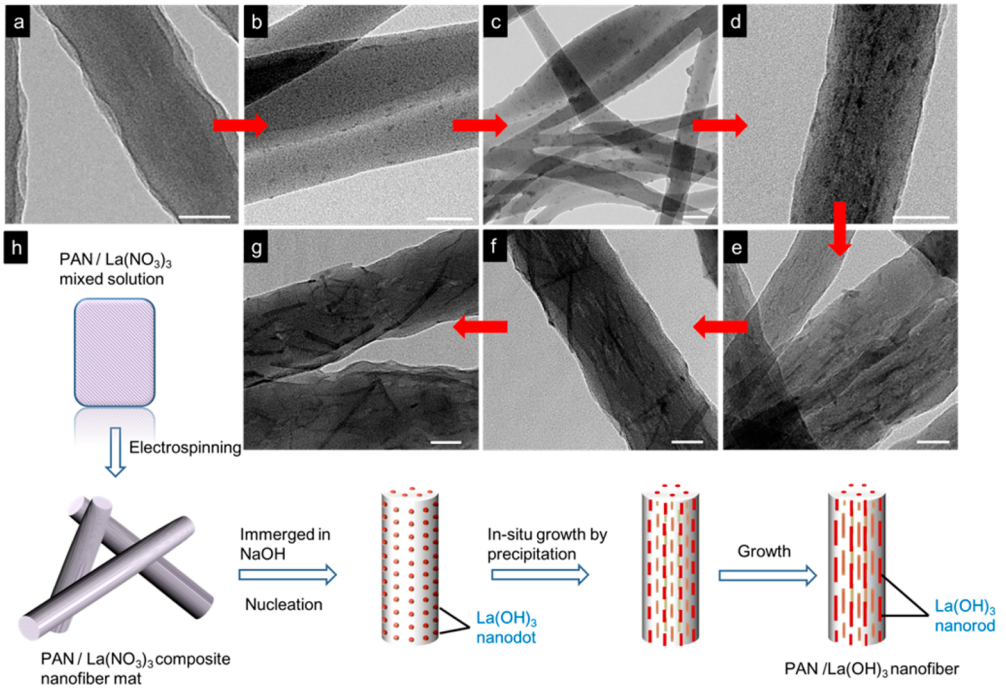

Figure 2. (a–f) TEM images of the composite nanofibers as a function of *in situ* treatment time by NaOH: (a) 0 min (PAN/$La(OH)_3$), (b) 30 min, (c) 1 h, (d) 2 h, (e) 6 h, (f) 10 h, (g) 12 h. The scale bar in the TEM images repesents 50 nm. (h) Scheme for the formation of dispersed-$La(OH)_3$ nanorods in PAN nanofibers by electrospinning and the subsequent *in situ* precipitation.

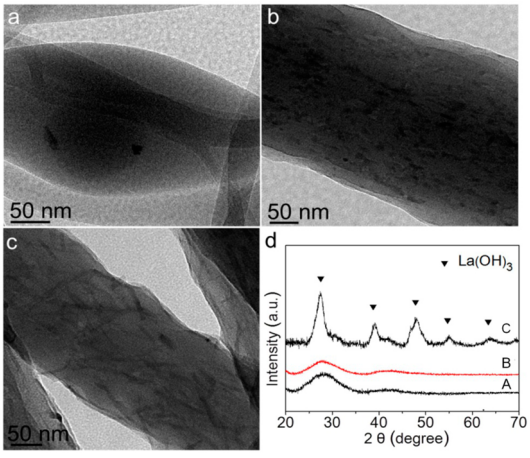

Figure 3. TEM images of PAN/$La(OH)_3$ nanofibers prepared by electrospinning and *in situ* precipitation. Initial mass ratios of PAN to $La(NO_3)_3 \cdot 6H_2O$: (a) 10:1, (b) 6:1 and (c) 3:1, respectively. (d) Lines A, B, and C in the XRD spectra represent the samples shown in (a), (b), and (c), respectively.

10:1, only a few $La(OH)_3$ nanoparticles appeared in PAN (Figure 3a). As the ratio changed into 6:1, more nanoparticles emerged and tended to agglomerate along a 1D direction (Figure 3b). The XRD spectra of the three samples are shown in Figure 3d. The lower the concentration of initial La^{3+} the more amorphous the $La(OH)_3$ crystal structures tended to be. On the basis of the data exhibited in Figures 2 and 3, it can be deduced that the growth of crystal $La(OH)_3$ nanorods in PAN nanofibers was both time-dependent and La concentration-dependent.

TABLE 1. Comparison of the Leakage of Lanthanum of Various Samples[a,b]

absorbents	leakage of lanthanum (μg/L)	immersion time (h)
PLNFs (Figure 3cFigure 3b)	ND[c]	24
PAN/$La(OH)_3$ particle (6:1) (Figure 3b)	3	1
PAN/$La(OH)_3$ particle (10:1) (Figure 3a)	5	1
$La(OH)_3$ nanocrystal (Figure 1e)	117	1

[a] Operating temperature 25 °C and initial phosphate concentration: 2 mg P/L. [b] The La dosage in the solutions was the same for the four samples. [c] Below the MDLs (1 μg La/L).

Phosphate Removal. We first evaluated the phosphate adsorption properties of the above three fiber samples with various La contents and found insignificant differences between the P capture abilities per gram La of each sample (Figure S4). The PLNFs with $La(OH)_3$ nanorods impregnated in PAN nanofibers exhibited much better resistance to La leaking during application (Table 1) than the other two samples and, thus, were chosen as the right sample to conduct the following phosphate adsorption and antibacterial experiments. Pure PAN nanofibers were used as a control sample for comparison, with a negligible phosphate adsorption capacity of only 0.277 mg/g (T = 25 °C, initial concentration = 50 mg P/L), indicating the removal capacities were nearly all derived from $La(OH)_3$ nanorods in PLNFs. Figure 4a showed Langmuir and Freundlich adsorption isotherms of PLNFs in the solution with different initial phosphate concentrations. The corresponding isotherm

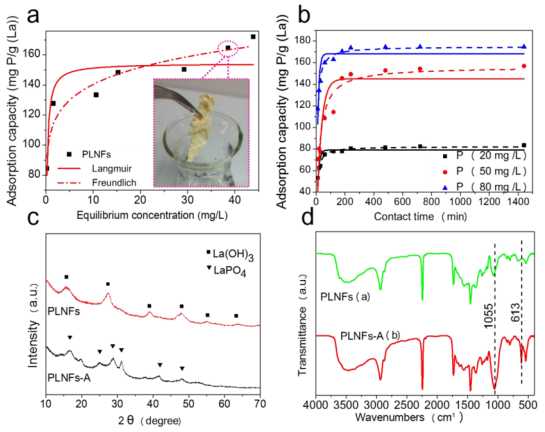

Figure 4. (a) The adsorption isotherms of the phosphate on the PLNFs (initial concentration = 20, 30, 40, 50, 60, 70, 80 mg P/L) (Inset: separation of adsorbents from solution after adsorption.) (b) Adsorption kinetics of the phosphate on PLNFs (initial concentration = 20, 50, 80 mg P/L). The above experiments were carried out at $T = 25$ °C without pH adjustment. (c) XRD patterns and (d) FT-IR spectra of the PLNFs before and after adsorption (PLNFs-A).

parameters are summarized in Table S1. The Freundlich model gave a better fit than the Langmuir model for the PLNFs with a correlation coefficient of $R^2 = 0.903$, indicating a chemical heterogeneity of the adsorbents. This result was different from other previous studies on lanthanum-based adsorbents,[29,50,51] likely caused by the aeolotropic structure of the $La(OH)_3$ nanorods in the nanofiber matrix.[52] On average, a favorable adsorption tended to have a Freundlich constant n between 1 and 10. A larger value of n implied a stronger interaction between adsorbents and phosphate.[53] For our adsorbent, n was 8.90 as shown in Table S1, representing a favorable adsorption condition.[54] Given that PAN did not contribute to the total adsorption capacity, and the $La(OH)_3$ content in the composite nanofibers was 7.8 wt %, the maximum phosphate adsorption capacity (q_m) of the PLNFs can thus be determined to be 172.2 mg P/g (La) ($T = 25$ °C) in the 80 mg P/L phosphate solution. This value was much higher than the maximum adsorption capacity of 20.4 mg P/g (La) for $La(OH)_3$ nanocrystals fabricated by CPM without PAN protection under the same experimental conditions and also higher than the saturated adsorption capacity of 76.8 mg P/g (La) for commercial nano-$La(OH)_3$.[29] It could be interpreted that the well-dispersed $La(OH)_3$ nanorods in the nanofibers brought more exposed $La(OH)_3$ active sites for phosphate binding.[55] Significantly, the adsorbent of PLNFs was very convenient to be separated from the solution after adsorption (Figure 4a, inset), owing to the good mechanical properties (Figure S5 and Table S2).

The time-dependent adsorption for high concentration phosphate is shown in Figure 4b. The phosphate removal was quite rapid at the initial stage, with >90% phosphate removed from the solution with 20 mg P/L by PLNFs in 1.5 h, and experiments under

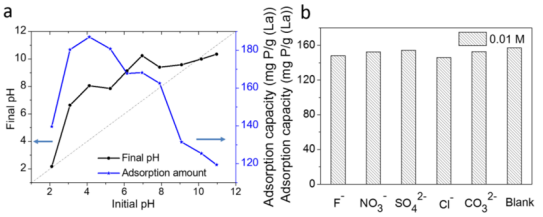

Figure 5. (a) Effect of initial pH on phosphate adsorption of PLNFs and the final pH variation of solution. (b) Effect of coexisting anions on the phosphate adsorption capacity.

different phosphate concentrations (20, 50, 80 mg P/L) could all reach equilibrium (>97%) within 6 h. The kinetic parameters as well as corresponding correlation coefficients are shown in Table S3. According to correlation coefficient R^2, the data fitted well to the pseudo-second-order rate equation, indicating a chemisorption process of the adsorption.[23]

The structures of lanthanum component in the functionalized composites after adsorption were investigated by wide-angle XRD (Figure 4c). Several characteristic peaks appeared at 2θ = 17.0°, 25.0°, 28.5°, 31.1°, and 41.9° after removal of phosphate, which corresponded to the monoclinic $LaPO_4$ phase (PDF no. 73-0188), confirming the chemical reaction between the adsorbed phosphate and the La active sites.[21,50] Meanwhile, Figure 4d presents the FT-IR spectra of the as-prepared PLNFs and PAN/$La(OH)_3$ nanofibers after adsorption (PLNFs-A). The obviously strengthened adsorption peak centered at about 1055 cm^{-1} should be attributed to the typical characteristic of the asymmetric stretch vibration of P—O in PLNFs-A. Additionally, the reduced intensity of the La—O—H peak at 635 cm^{-1} (Figure S6)[56] and the appearance of the O—P—O peak at 613 cm^{-1} also suggested the chemical binding between La and phosphate.[57] The morphology and chemical compositions of PLNFs-A were also studied by TEM and SAED, supplied in Figure S7 in the Supporting Information. The lanthanum species in PAN nanofibers retained 1D nanostructure after adsorption of phosphate.

The effect of the pH, ranging from 2.0 to 11.0, on the phosphate uptake capacities of the monodispersed $La(OH)_3$ in the PAN nanofibers were investigated and areshown in Figure 5a. The phosphate removal properties, kept at a high level in the pH range of 3.0—8.0, indicated a wide application. In faintly acid solution, the protonation of the samples was expected to make the surface of $La(OH)_3$ positively charged, consequently facilitating the interaction with anionic group $H_2PO_4^-$ or HPO_4^{2-} by electrostatic attraction to form $LaPO_4$.[50,58] Additionally, the ligand-exchange mechanism would also be involved in the phosphate adsorption process following eqs 1—3, responsible for the high adsorption capacities,[50,51,58] which could be confirmed by the obvious increases in pH value (ΔpH = final pH − initial pH) during the adsorption

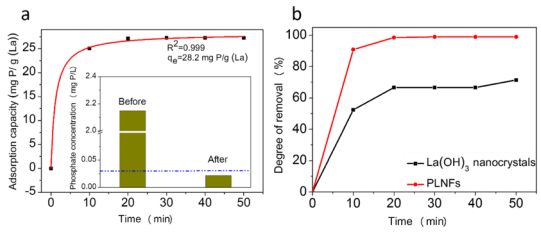

Figure 6. (a) Phosphate adsorption in the synthetic solution by using PLNFs. (b) Comparison of removal percentage over PLNFs and La(OH)$_3$ nanocrystals by CPM, respectively.

process (Figure 5a).

$$La-OH + H_2PO_4^- \rightleftharpoons La-H_2PO_4 + OH^- \quad (1)$$

$$La{=}(OH)_2 + HPO_4^{2-} \rightleftharpoons La{=}HPO_4 + 2OH^- \quad (2)$$

$$La{\equiv}(OH)_3 + PO_4^{3-} \rightleftharpoons La{\equiv}PO_4 + 3OH^- \quad (3)$$

When the pH value increased further from 8.0 to 11.0, the higher OH^- concentration worked against the aforementioned reactions of eqs 1−3, in turn resulting in a sharp decrease in phosphate removal capacity. It was also observed that when the pH was below 3.0 the phosphate adsorption capacities were relatively low. It should be noted that when pH ≤ 3 H_3PO_4 that could not be adsorbed by La(OH)$_3$[57,59] and reached a higher concentration.

Phosphate competitive adsorption studies (Figure 5b) of the PLNFs were carried out in the presence of common ions like F^-, Cl^-, SO_4^{2-}, CO_3^{2-}, and NO_3^- in water. There was no obvious influences on adsorption capacity (q_e) by adding 0.01 M coexisting anions into 50 mg P/L phosphate solution, suggesting a high selective phosphate removal capacity of PLNFs with strong anti-interference ability.

Removal of Low Concentration Phosphate. The treatment of the phosphate faces a thorny problem in that possible abnormal growth of microorganism occurs at a very low phosphate concentration. Some countries even use 0.03 mg P/L to prevent water from blooms of cyanobacteria.[26,60] Thus, it is necessary to assess the removal properties of our agent toward low concentration phosphate. Herein, to study the practical feasibility of our fabricated PLNFs, we conducted an adsorption test in synthetic solution with an initial phosphate (P) concentration of 2 mg P/L.[61−63] The PLNFs exhibited a very fast adsorption, with 90.9% of phosphate removed within the first 10 min and 98.9% within 20 min. The residual phosphate concentration in the solution is 22 μg P/L after 20 min treatment by PLNFs, which was below the phosphate limits of some countries (30 μg P/L, the dash line showed in Figure 6a). Furthermore, the data were well fitted to the pseudo-second-order model and with a correlation coefficient R^2 = 0.999. The phosphate removal percentage over PLNFs and La(OH)$_3$ nanocrystal by CPM were compared in Figure 6b, and the La dosage was the same in water for these two samples. There was only 71.4% phosphate removed after 50 min by La(OH)$_3$ nanocrystals, and the total removal percentage by this sample reached just 85.7% after 24 h. These results suggested that the super high-speed adsorption ability of PLNFs should be owing to the well-dispersed construction of La(OH)$_3$ nanorods in PAN nanofibers. The results implied a great application potential of the PLNFs as chemical treatment agents to decrease the phosphate concentration for more stringent discharge limit.

The leakage problem is a bottleneck that hinders conventional La-containing materials for practical application, such as drinking water treatment and antibacteria.[64,65] In order to monitor the amounts of La released from PLNFs, the leakage was detected by ICP-OES after PLNFs (1 g/L) were immerged in phosphate solution (2 mg P/L) for 24 h. The results showed that the released lanthanum concentration was below the MDLs (method detection limits) of ICP-OES (1 μg La/L), comparable to the lanthanum content in open waters (<1 μg La/L).[3] In previous works, researchers also developed methods to protect La from leaking, *e.g.*, using mesoporous or macroporous silica to stabilize the La species. However, the residual lanthanum in water released from those materials were hundreds or thousands times higher than that of PLNFs.[24,26] Two reasons are proposed to explain the PLNFs' excellent resistance to leaking. The main one is that *in situ* immobilization by PAN nanofibers can not only make the La(OH)$_3$ easily separated out after reactions, but also effectively avoid La leaking. This can be supported by the control experiment that the released lanthanum concentration from pure La(OH)$_3$ nanocrystals in 1 h was as high as 117 μg La/L (Table 1). The other possible reason may be related to the higher aspect ratio of the 1D crystalline La(OH)$_3$ nanorods. It should be more difficult for 1D nanostructure to divorce from PAN encapsulation due to the larger steric hindrance than that of nanoparticles. It can be supplied by the data shown in Table 1, for the other two PAN/La(OH)$_3$ with nanoparticles in PAN nanofibers (the sample depicted in Figure 3a,b), the La residue in solution in 1 h was more than 3 times that of PLNFs even in 24 h.

Phosphate Starvation Antibacteria. In order to demonstrate the antimicrobial strategy by phosphate starvation, the antibacterial property of PLNFs against *Escherichia coli* (*E. coli*) was investigated. The solution with an initial phosphate concentration of 2 mg P/L was first pretreated by PLNFs (1.0 g/L) for 20 min and then mixed with *E. coli* and used as the media for microbe growth. To illustrate the impact of the phosphate scavenging influence on the antibacterial property, the phosphate solution without preadsorption by PLNFs was employed as a control sample. As shown in Figure 7a, bacterial contamination (CFU per milliliter) was found at the same level for the two samples at the

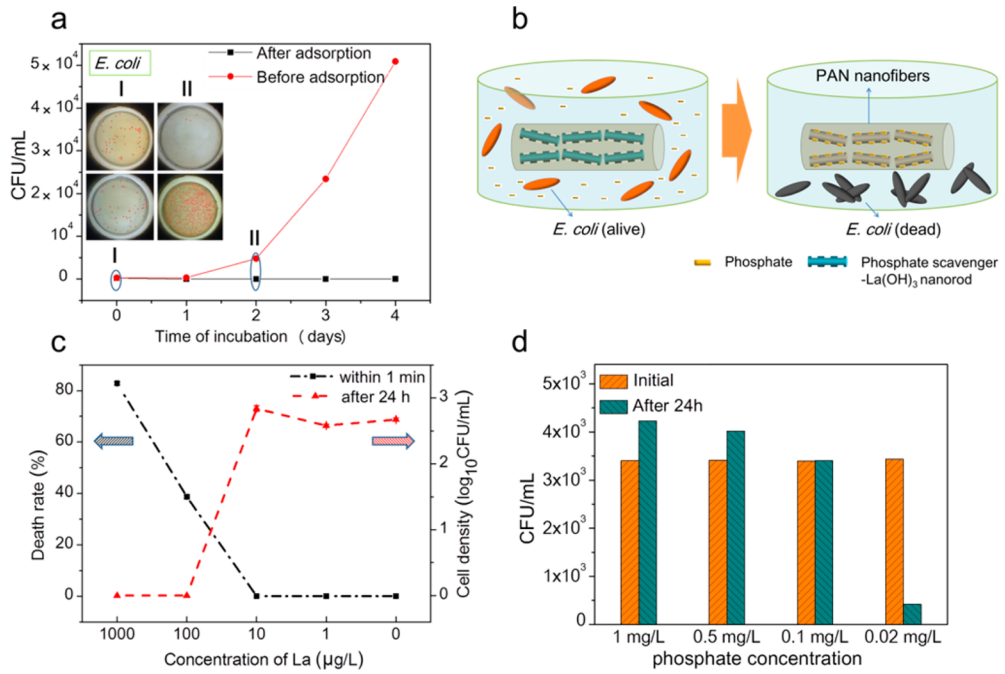

Figure 7. (a) *E. coli* growth processes in water with 2 mg P/L phosphate (red line) and in that pretreated by PLNFs (black line). Once the media and organism were mixed, 250 μL of each sample was spread on the LB solid medium plates as the 0 day sample. During 4 days no growth was observed in the phosphate-free water, while bacteria rapidly colonized water under adequate phosphate conditions. (Inset: colonies on agar plates corresponding to the samples of (I) 0 day and (II) second day.) (b) Schematic illustration of the nutrient-starvation antibacteria by PLNFs. (c) Antibacterial activities of free La^{3+} ions at various concentrations: 90 μL of *E. coli* (about 10^8 CFU/mL) were incubated with 150 mL of La^{3+} solution. (d) Cell viability after incubation with different phosphate concentrations (1, 0.5, 0.1 mg P/L and 0.02 mg P/L).

beginning, 216 CFU/mL for the sample without pre-adsorption and 192 CFU/mL for the adsorbed sample. Then, the *E. coli* colony in the media treated by PLNFs showed a severe slash, completely dead within 1 day (8 CFU detectable in 1 mL solution) and remained stable at 8 CFU/mL even after 4 days of incubation. On the contrary, evident growth occurred under phosphate conditions after 1 day (316 CFU/mL), 2 days (4790 CFU/mL, Figure 7a), and 4 days (50900 CFU/mL) of incubation. The result suggests the excellent persistent antibacterial activity of PLNFs. According to the above-mentioned experiments, the antimicrobial mechanism of the PLNFs is speculated as nutrient starvation. The strong binding of the lanthanum hydroxide nanorods in the PAN fibers with phosphate caused the shortage of the essential element for the survival and growth of microorganisms (Figure 7b).

To ensure the phosphate-starvation antibacterial mechanism of La-based materials, the direct antibacterial effect of released La^{3+} must be ruled out first. The *E. coli* death rate in solutions containing different concentrations of lanthanum nitrate were measured and compared in Figure 7c. It was found that La^{3+} with higher concentration exhibited a fast and high inhibition to the bacteria. The death rates of *E. coli* were around 83% and 39% within 1 min in the solution with 1000 and 100 μg/L La^{3+}, respectively. However, there was no observable cell death in pure ddH_2O and other La^{3+} solutions with lower concentration (10 μg/L and 1 μg/L) within 1 min. After incubation for 24 h, the density of *E. coli* under the above five conditions decreased because there was no phosphate added in. All of the bacteria were dead when the La^{3+} concentration was higher than 100 μg/L. But for the 1 μg/L and 10 μg/L La^{3+} solutions, the density of survival *E. coli* was about several hundred CFU/mL, the same level as that in pure water. This study indicates that there is no remarkable direct antibacterial effect of La^{3+} when the concentration is below 10 μg/L. In the present work, the leaked lanthanum from PLNFs into water was below <1 μg/L; thus, the antimicrobial mechanism of the PLNFs was reasonably proposed to be nutrient starvation.[21] Moreover, the cell activities in phosphate solution of various concentrations without any antibacterial agents were also evaluated and are provided in Figure 7d. When the phosphate concentration was 0.02 mg P/L, the media exhibited high antibacterial activities due to the absence of nutrition. This result can further confirm the phosphate-starvation antibacterial mechanism of PLNFs, because the phosphate residue was 0.022 mg P/L after 20 min pretreatment by PLNFs (Figure 6b). As the P concentration was beyond 0.1 mg P/L, the aqueous media was biocompatible for bacterial survival or growth. It indicated that the control sample of pure $La(OH)_3$ nanocrystals, with phosphate residue more than 0.5 mg P/L, was not effective for killing *E.coli* by phosphate starvation when the La dosage was the same as that of PLNFs.

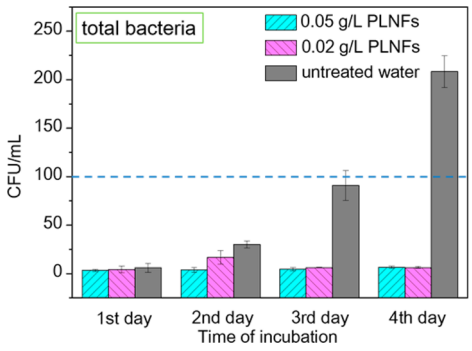

Figure 8. Investigation of biostability of real drinking water samples against being recontaminated by total bacteria. Three sterilized tap water samples were all incubated in an indoor environment, with two exposed, respectively, to 0.02 g/L and 0.05 g/L PLNFs for 1 h every day and the other one without treatment by PNLFs.

Water Biostability against Being Recontaminated by Total Bacteria. *E. coli* is not the only bacterial species in water. Therefore, considering practical application, it is quite necessary to estimate the antibacterial efficiency of PLNFs toward total bacteria in real water samples. Fresh tap water was first taken from a sterilized tap and then placed in a sterile environment for days to release some residual chlorine. Then the above water sample was divided into three parts and incubated in indoor environment, with one part serving as a blank sample and the other two parts exposed to 0.02 g/L and 0.05 g/L PLNFs, respectively, for 1 h in each of the following days. It is clearly observed from Figure 8 that the bacteria colony number of the untreated water displayed a remarkably increase from ~10 CFU/mL to 200 CFU/mL, exceeding the Standard for Drinking Water Quality of China and World Health Organization (<100 CFU/mL) within 3 days. It indicates that rapid bacterial recontamination can occur even in sanitized water. In contrast, the other two samples guaranteed by the PLNFs kept the number of standard plate-count bacteria steady at around 10 CFU/mL, confirming the validity of PLNFs to suppress the regrowth of bacteria in real drinking water. Even though various forms of phosphorus compounds exist in water, it is widely accepted that phosphate is the only form of P that can be directly assimilated by microorganism, algae and other planktons.[14] PLNFs, as a vigorous competitor to bind phosphate, can block the metabolism of the cells through the rapid P uptake, thus preventing the recontamination.[27] Therefore, PLNFs is foreseen to possess great application prospects in securing biological stability in water production, supply, as well as storage.

CONCLUSIONS

In summary, well-dispersed-$La(OH)_3$ nanorods were *in situ* impregnated in PAN nanofibers by combining electrospinning with a surfactant-free precipitation process. PAN nanofibers acted as not only a growth controller but also an agglomeration inhibitor for the formation of the $La(OH)_3$ aeolotropic nanostructures. Compared with conventional $La(OH)_3$ nanostructures, the hierarchically nanostructured PLNFs exhibited a fast kinetics, high-removal rate, and easy separation for phosphate adsorption, even toward low concentration targets. This benefited from the increased active sites, which were provided by the well-dispersed $La(OH)_3$ nanorods to chemically bind with phosphate. Finally, an effective nutrient-starvation antibacteria strategy was successfully demonstrated through scavenging free bioavailable phosphate by PLNFs, and kept water biostable. Considering that the *in situ* encapsulation by PAN nanofibers can both avoid lanthanum leakage and bring out higher removal efficiency toward nutrient, the present work would be of particular interest for antibacteria and water stability in practical application. In addition, due to the important role of one-dimensional lanthanide hydroxides, the present work may also find important applications in catalysis, optical devices and electronics, *etc*.

MATERIALS AND METHODS

Materials. *N,N*-Dimethylformamide (DMF) and lanthanum nitrate ($La(NO_3)_3 \cdot 6H_2O$) were provided by Aladdin Chemical Reagent Co., Ltd. (Shanghai, China). Sodium hydroxide (NaOH) was purchased from Sinopharm Chemical Reagent Co., Ltd. (Beijing, China). Polyacrylonitrile (PAN) (M_w = ~ 80,000) was used as received from Jilin Carbon Group, China. All of the chemical reagents used were analytical grade. *E. coli.* (ATCC 25922) was incubated via the previous procedure reported in literature.[26]

Fabrication and Characterization of the Composite Nanofibers. PAN (5 wt %) and certain amounts of $La(NO_3)_3 \cdot 6H_2O$ were dissolved in DMF, under vigorous stirring at 80 °C for 3 h. The mass ratios of PAN to $La(NO_3)_3 \cdot 6H_2O$ in various samples were 3:1, 6:1 and 10:1, respectively. After being cooled to room temperature, the above mixtures were loaded into a plastic syringe for electrospinning. An electric potential of 15 kV was applied between the orifice and the ground at a distance of 20 cm, with a feed rate of 0.1 mL/h by a syringe pump (Fisher Scientific, USA) under ambient conditions (environmental humidity <50%). Then, the as-prepared precursor nanofibers were treated by 0.1 M NaOH for 12 h at room temperature to *in situ* convert $La(NO_3)_3$ in PAN nanofibers into $La(OH)_3$, which is called the *in situ* precipitation method. Finally, the products were dried in a vacuum oven at 45 °C for 24 h after washed by deionized water for more than 10 times.

For comparison, pure PAN nanofibers were also fabricated by electrospinning without addition of $La(NO_3)_3 \cdot 6H_2O$. Pure $La(OH)_3$ nanocrystals were prepared by a conventional precipitation method, concerning a reaction between NaOH and $La(NO_3)_3$ solution, without addition of PAN or any organic surfactant.

FT-IR spectra of the samples were recorded on a PerkinElmer Spectrum One B spectrometer with KBr as the reference. The crystal structure of the samples was investigated using an X-ray diffraction (XRD) by Bruker D8 Advance diffractometer in the range of 2θ = ~90° using Cu Kα radiation as X-ray source. The microstructures of the products were observed on a Helios

Nanolab600i field emission scanning electron microscope (FE-SEM). High resolution transmission electron microscope (HRTEM) imaging analysis was performed with a FEI Tecnai G2 F30, operated at a 300 kV accelerating voltage. The lanthanum contents in PAN/$La(OH)_3$ nanofibers were detected by using an inductively coupled plasma optical emission spectrometer (ICP-OES, Optima 5300 DV, PerkinElmer). The samples for ICP-OES were prepared by digesting 0.1 g of products with 6 mL of HNO_3, 2 mL of $HClO_4$ and 2 mL of HCl, followed by dilution with 2% HNO_3.

Characterization of the Phosphate Removal Properties of the Composite Nanofibers. A batch of tests were conducted to investigate the phosphate adsorption capability of the pure PAN nanofibers, pure $La(OH)_3$ nanocrystal and PLNFs. Phosphate solutions were prepared by dissolving potassium dihydrogen phosphate (KH_2PO_4) in DI water. All the experiments were carried out at 25 °C in 150 mL conical flask at the shaken rate of 130 rpm for 24 h. Phosphate solution (50 mL) was used for each experiment with 3.0 g/L of adsorbents suspended in it.

As for the equilibrium studies, the adsorbents were added in the solutions with initial phosphate concentration ranging from 20 to 80 mg P/L. Langmuir and Freundlich equations were applied to describe the adsorption isotherm data by nonlinear regression forms[57]

$$q_e = q_m K_L C_e/(1 + K_L C_e) \quad (4)$$

$$q_e = K_F C_e^{1/n} \quad (5)$$

where C_e (mg/L) is the concentration of phosphate solution at equilibrium, q_e (mg/g) is the corresponding adsorption capacity, q_m (mg/g) and K_L (L/mg) are Langmuir constants related to adsorption capacity and energy or net enthalpy of adsorption, respectively, and K_F (mg/g) and n are the Freundlich constants.

For the adsorption kinetic experiments, 3.0 g/L of PLNFs was added in the solution containing initial phosphate concentrations of 20, 50, and 80 mg P/L. Then 2 mL solution was taken out of the flask at given time intervals for phosphate concentration analysis. In order to analyze the kinetic mechanism of the adsorption process, the experimental data were fitted in the pseudo-first-order and pseudo-second-order models, which are described as the following equations[51]

$$\text{pseudo first-order equation}: \ln(q_e - q_t) = \ln q_e - k_1 t \quad (6)$$

$$\text{pseudo-second-order equation}: t/q_t = 1/(k_2 q_e^2) + t/q_e \quad (7)$$

where q_t and q_e are the amount of phosphate adsorbed over a given period of time t (mg P/g) and at equilibrium (mg P/g), respectively; t is the adsorption time (min); and k_1 (1/min) and k_2 ($g \cdot mg^{-1}min^{-1}$) are the adsorption rate constant of the pseudo-first-order adsorption and the pseudo-second-order adsorption, respectively.

To study the pH effect on phosphate removal, PLNFs were added into 50 mg P/L phosphate solution. The initial pH, ranging from 2.0 to 11.0, was adjusted by NaOH and/or HCl solutions. The effect of coexisting anions on phosphate adsorption capacities was evaluated by dissolving 0.01 M of F^-, NO_3^-, SO_4^{2-}, Cl^- and CO_3^{2-} into 50.0 mL of phosphate solution with an initial concentration of 50.0 mg P/L.

The adsorption experiment toward low concentration phosphate was conducted in a solution with 2 mg/L by using potassium dihydrogen phosphate as sources. The dosage of the PLNFs was 1.0 g/L in this experiment. $La(OH)_3$ nanocystals fabricated by CPM served as a control sample, with the same La dosage as that in the PLNFs.

The concentrations of the phosphate solutions were determined by using the Ammonium molybdate spectrophotometric method.[58] The absorption properties of the samples were characterized by UV–vis spectrophotometer (Shanghai Metash Instruments Co., Ltd., China). The pH of the solution was analyzed by Sartorius PB-10 (Sartorius, Germany). The concentration of lanthanum ion leakage was analyzed by using ICP-OES.

Phosphate-Starvation Antibacterial toward *E. coli*. To demonstrate the nutrient starvation antibacterial strategy, 2 mg P/L phosphate solutions with and without pretreatment by 1.0 g/L PLNFs (20 min) were both employed to serve as the media for organism growth. The solutions were sterilized by autoclaving at 121 °C for 30 min before the experiments.

E. coli cells were chosen as target microbes and cultivated at 37 °C in Luria–Bertani (LB) medium overnight first. Until the colony grew beyond 10^8 CFU/mL, the suspension was centrifuged (Mistral 3000E, 3000 rpm) for 10 min and washed with physiological saline (0.9 wt % NaCl in water) to remove the nutrient from LB medium (5 times repeatedly). Then the microbes were diluted to 10^3–10^4 CFU/mL, and 2 mL was taken out to add into the as-prepared solutions (0.5 mL, 10 mg P/L) and incubated at 37 °C in 5 mL centrifuge tubes on a shaker (150 rpm). 250 μL of each sample was spread on the agar (LB) plates every day. The plates were incubated at 37 °C for 24 h before readout. The water used in microorganism experiments was all ddH_2O (Milli-Q, Millipore, resistivity 18 MΩ cm) and presterilized at 121 °C for 30 min.

To measure the impact of free La^{3+} ions on the growth of *E. coli*., 90 μL of *E. coli* (about 10^8 CFU/mL) was incubated with 150 mL of solutions containing various La^{3+} contents (1000, 100, 10, 1, and 0 μg/L) for 24 h at 37 °C. The cell viability in media with various phosphate concentration was tested by incubating 50 μL of bacterial suspensions (about 10^7 CFU/mL) with 50 mL of phosphate solution at different concentrations (1, 0.5, 0.1, and 0.02 mg P/L) for 24 h at 37 °C, and then 100 μL of the cell suspension was incubated onto LB agar plates.

Water Biostability against Being Recontaminated by Total Bacteria. The biostability of real water samples against being recontaminated by total bacteria was tested followed the standard examination method for drinking water in China (GB/T 5750-2006). The standard plate-count bacteria was chosen as the analysis object. The fresh water was taken from a sterilized tap and then placed in a sterile environment for 3 days to release some residual chlorine. Subsequently, the above water sample was divided into three parts and incubated in indoor environment, with one part serving as a blank test the other two parts being allowed to contact with 0.02 g/L and 0.05 g/L PLNF mats for 1 h in each of the following days, respectively. A 100 μL portion of each sample was spread on the beef extract peptone agar plates every day and then incubated at 37 °C for 48 h before readout.

Conflict of Interest: The authors declare no competing financial interest.

Acknowledgment. We gratefully acknowledge the National Natural Science Foundation of China (Grant No. 21304024), State Key Laboratory of Urban Water Resource and Environment (Grant No. 2013TS06), Fundamental Research Funds for the Central Universities (Nos. 5710006113 and HIT.BRETIII.201417), Postdoctoral Science Foundation of China (Nos. 2014T70324 and LBH-Z12090), National Water Pollution Control and Treatment Science and Technology Major Project of China (Nos. 2012ZX07403004 and 2012ZX07408001), and Singapore National Research Foundation (CREATE Programme of Nanomaterials for Energy and Water Management).

Supporting Information Available: The Supporting Information is available free of charge on the ACS Publications website at DOI: 10.1021/acsnano.5b04236.

Photograph, SEM, low-magnification TEM image and diameter distribution of PLNFs; diameter distribution of $La(OH)_3$ nanorods in PLNFs after being immerged in NaOH for 12 and 10 h; adsorption capacities of various PAN/$La(OH)_3$ nanofibers with initial mass ratios of PAN to $La(NO_3)_3 \cdot 6H_2O$ of 10:1, 6:1, and 3:1, respectively; FT-IR spectra of $La(OH)_3$ nanocrystals; morphology and structure of PLNFs after adsorption; mechanical properties of PLNFs; the data of equilibrium experiments and adsorption kinetic experiments (PDF)

REFERENCES AND NOTES

1. Jones, K. E.; Patel, N. G.; Levy, M. A.; Storeygard, A.; Balk, D.; Gittleman, J. L.; Daszak, P. Global Trends in Emerging Infectious Diseases. *Nature* **2008**, *451*, 990–993.

2. Yin, S.; Goldovsky, Y.; Herzberg, M.; Liu, L.; Sun, H.; Zhang, Y.; Meng, F.; Cao, X.; Sun, D. D.; Chen, H.; et al. Functional Free-Standing Graphene Honeycomb Films. *Adv. Funct. Mater.* **2013**, *23*, 2972–2978.
3. Rotzetter, A. C. C.; Kellenberger, C. R.; Schumacher, C. M.; Mora, C.; Grass, R. N.; Loepfe, M.; Luechinger, N. A.; Stark, W. J. Combining Phosphate and Bacteria Removal on Chemically Active Filter Membranes Allows Prolonged Storage of Drinking Water. *Adv. Mater.* **2013**, *25*, 6057–6063.
4. Irwansyah, I.; Li, Y.; Shi, W.; Qi, D.; Leow, W. R.; Tang, M. B. Y.; Li, S.; Chen, X. Gram-Positive Antimicrobial Activity of Amino Acid-Based Hydrogels. *Adv. Mater.* **2015**, *27*, 648–654.
5. Xiong, M.; Li, Y.; Bao, Y.; Yang, X.; Hu, B.; Wang, J. Bacteria-Responsive Multifunctional Nanogel for Targeted Antibiotic Delivery. *Adv. Mater.* **2012**, *24*, 6175–6180.
6. Ng, V. W. L.; Ke, X.; Lee, A. L. Z.; Hedrick, J. L.; Yang, Y. Y. Synergistic Co-Delivery of Membrane-Disrupting Polymers with Commercial Antibiotics against Highly Opportunistic Bacteria. *Adv. Mater.* **2013**, *25*, 6730–6736.
7. Strassert, C. A.; Otter, M.; Albuquerque, R. Q.; Höne, A.; Vida, Y.; Maier, B.; De Cola, L. Photoactive Hybrid Nanomaterial for Targeting, Labeling, and Killing Antibiotic-Resistant Bacteria. *Angew. Chem., Int. Ed.* **2009**, *48*, 7928–7931.
8. Li, P.; Zhou, C.; Rayatpisheh, S.; Ye, K.; Poon, Y. F.; Hammond, P. T.; Duan, H.; Chan-Park, M. B. Cationic Peptidopolysaccharides Show Excellent Broad-Spectrum Antimicrobial Activities and High Selectivity. *Adv. Mater.* **2012**, *24*, 4130–4137.
9. Agnihotri, S.; Mukherji, S.; Mukherji, S. Immobilized Silver Nanoparticles Enhance Contact Killing and Show Highest Efficacy: Elucidation of The Mechanism of Bactericidal Action of Silver. *Nanoscale* **2013**, *5*, 7328–7340.
10. Gagnon, J.; Clift, M. J. D.; Vanhecke, D.; Kuhn, D. A.; Weber, P.; Petri-Fink, A.; Rothen-Rutishauser, B.; Fromm, K. M. Integrating Silver Compounds and Nanoparticles into Ceria Nanocontainers for Antimicrobial Applications. *J. Mater. Chem. B* **2015**, *3*, 1760–1768.
11. Gunawan, P.; Guan, C.; Song, X.; Zhang, Q.; Leong, S. S. J.; Tang, C.; Chen, Y.; Chan-Park, M. B.; Chang, M. W.; Wang, K.; et al. Hollow Fiber Membrane Decorated with Ag/MWNTs: toward Effective Water Disinfection and Biofouling Control. *ACS Nano* **2011**, *5*, 10033–10040.
12. Liu, S.; Wei, L.; Hao, L.; Fang, N.; Chang, M. W.; Xu, R.; Yang, Y.; Chen, Y. Sharper and Faster "Nano Darts" Kill More Bacteria: A Study of Antibacterial Activity of Individually Dispersed Pristine Single-Walled Carbon Nanotube. *ACS Nano* **2009**, *3*, 3891–3902.
13. Lürling, M.; Oosterhout, F. V. Controlling Eutrophication by Combined Bloom Precipitation and Sediment Phosphorus Inactivation. *Water Res.* **2013**, *47*, 6527–6537.
14. Correll, D. L. The Role of Phosphorus in The Eutrophication of Receiving Waters: A Review. *J. Environ. Qual.* **1998**, *27*, 261–266.
15. Chen, L.; Zhao, X.; Pan, B.; Zhang, W.; Hua, M.; Lv, L.; Zhang, W. Preferable Removal of Phosphate from Water Using Hydrous Zirconium Oxide-Based Nanocomposite of High Stability. *J. Hazard. Mater.* **2015**, *284*, 35–42.
16. Guaya, D.; Valderrama, C.; Farran, A.; Armijos, C.; Cortina, J. L. Simultaneous Phosphate and Ammonium Removal from Aqueous Solution by A Hydrated Aluminum Oxide Modified Natural Zeolite. *Chem. Eng. J.* **2015**, *271*, 204–213.
17. Lv, J.; Yuan, L.; Chen, X.; Liu, L.; Luo, D. Phosphorus Metabolism and Population Dynamics in A Biological Phosphate-Removal System with Simultaneous Anaerobic Phosphate Stripping. *Chemosphere* **2014**, *117*, 715–721.
18. Autissier, V.; Damment, S. J. P.; Henderson, R. A. Relative *in vitro* Efficacy of The Phosphate Binders Lanthanum Carbonate and Sevelamer Hydrochloride. *J. Pharm. Sci.* **2007**, *96*, 2818–2827.
19. Spears, B. M.; Lürling, M.; Yasseri, S.; Castro-Castellon, A. T.; Gibbs, M.; Meis, S.; McDonald, C.; McIntosh, J.; Sleep, D.; Van Oosterhout, F. Lake Responses Following Lanthanum-Modified Bentonite Clay (Phoslock®) Application: An Analysis of Water Column Lanthanum Data from 16 Case Study Lakes. *Water Res.* **2013**, *47*, 5930–5942.
20. Lürling, M.; Tolman, Y. Effects of Lanthanum and Lanthanum-Modified Clay on Growth, Survival and Reproduction of Daphnia Magna. *Water Res.* **2010**, *44*, 309–319.
21. Yang, J.; Zhou, L.; Zhao, L.; Zhang, H.; Yin, J.; Wei, G.; Qian, K.; Wang, Y.; Yu, C. A Designed Nanoporous Material for Phosphate Removal with High Efficiency. *J. Mater. Chem.* **2011**, *21*, 2489–2494.
22. Zhang, J.; Shen, Z.; Shan, W.; Chen, Z.; Mei, Z.; Lei, Y.; Wang, W. Adsorption Behavior of Phosphate on Lanthanum(III) Doped Mesoporous Silicates Material. *J. Environ. Sci.* **2010**, *22*, 507–511.
23. Zhang, J.; Shen, Z.; Shan, W.; Mei, Z.; Wang, W. Adsorption Behavior of Phosphate on Lanthanum(III)-Coordinated Diamino-Functionalized 3D Hybrid Mesoporous Silicates Material. *J. Hazard. Mater.* **2011**, *186*, 76–83.
24. Ou, E.; Zhou, J.; Mao, S.; Wang, J.; Xia, F.; Min, L. Highly Efficient Removal of Phosphate by Lanthanum-Doped Mesoporous SiO_2. *Colloids Surf., A* **2007**, *308*, 47–53.
25. Shin, E. W.; Karthikeyan, K. G.; Tshabalala, M. A. Orthophosphate Sorption onto Lanthanum-Treated Lignocellulosic Sorbents. *Environ. Sci. Technol.* **2005**, *39*, 6273–6279.
26. Yang, J.; Yuan, P.; Chen, H.; Zou, J.; Yuan, Z.; Yu, C. Rationally Designed Functional Macroporous Materials as New Adsorbents for Efficient Phosphorus Removal. *J. Mater. Chem.* **2012**, *22*, 9983–9990.
27. Gerber, L. C.; Moser, N.; Luechinger, N. A.; Stark, W. J.; Grass, R. N. Phosphate Starvation as An Antimicrobial Strategy: The Controllable Toxicity of Lanthanum Oxide Nanoparticles. *Chem. Commun.* **2012**, *48*, 3869–3871.
28. Gibbs, M. M.; Hickey, C. W.; Özkundakci, D. Sustainability Assessment and Comparison of Efficacy of Four P-Inactivation Agents for Managing Internal Phosphorus Loads in Lakes: Sediment Incubations. *Hydrobiologia* **2011**, *658*, 253–275.
29. Xie, J.; Wang, Z.; Lu, S.; Wu, D.; Zhang, Z.; Kong, H. Removal and Recovery of Phosphate from Water by Lanthanum Hydroxide Materials. *Chem. Eng. J.* **2014**, *254*, 163–170.
30. Feng, L.; Xiao, H.; He, X.; Li, Z.; Li, F.; Liu, N.; Zhao, Y.; Huang, Y.; Zhang, Z.; Chai, Z. Neurotoxicological Consequence of Long-Term Exposure to Lanthanum. *Toxicol. Lett.* **2006**, *165*, 112–120.
31. Zhu, Y.; Han, X.; Xu, Y.; Liu, Y.; Zheng, S.; Xu, K.; Hu, L.; Wang, C. Electrospun Sb/C Fibers for A Stable and Fast Sodium-Ion Battery Anode. *ACS Nano* **2013**, *7*, 6378–6386.
32. Peng, S.; Li, L.; Hu, Y.; Srinivasan, M.; Cheng, F.; Chen, J.; Ramakrishna, S. Fabrication of Spinel One-Dimensional Architectures by Single-Spinneret Electrospinning for Energy Storage Applications. *ACS Nano* **2015**, *9*, 1945–1954.
33. Chen, M.; Besenbacher, F. Light-Driven Wettability Changes on A Photoresponsive Electrospun Mat. *ACS Nano* **2011**, *5*, 1549–1555.
34. He, D.; Hu, B.; Yao, Q.; Wang, K.; Yu, S. Large-Scale Synthesis of Flexible Free-Standing SERS Substrates with High Sensitivity: Electrospun PVA Nanofibers Embedded with Controlled Alignment of Silver Nanoparticles. *ACS Nano* **2009**, *3*, 3993–4002.
35. Chen, P.; Liang, H.; Lv, X.; Zhu, H.; Yao, H.; Yu, S. Carbonaceous Nanofiber Membrane Functionalized by beta-Cyclodextrins for Molecular Filtration. *ACS Nano* **2011**, *5*, 5928–5935.
36. Uyar, T.; Havelund, R.; Hacaloglu, J.; Besenbacher, F.; Kingshott, P. Functional Electrospun Polystyrene Nanofibers Incorporating α-, β-, and γ-Cyclodextrins: Comparison of Molecular Filter Performance. *ACS Nano* **2010**, *4*, 5121–5130.
37. Lee, J. S.; Kwon, O. S.; Park, S. J.; Park, E. Y.; You, S. A.; Yoon, H.; Jang, J. Fabrication of Ultrafine Metal-Oxide-Decorated Carbon Nanofibers for DMMP Sensor Application. *ACS Nano* **2011**, *5*, 7992–8001.
38. Yu, D.; Zhou, J.; Chatterton, N. P.; Li, Y.; Huang, J.; Wang, X. Polyacrylonitrile Nanofibers Coated with Silver Nanoparticles Using A Modified Coaxial Electrospinning. *Int. J. Nanomed.* **2012**, *7*, 5725–5732.
39. Nataraj, S. K.; Yang, K. S.; Aminabhavi, T. M. Polyacrylonitrile-Based Nanofibers—A State-of-The-Art Review. *Prog. Polym. Sci.* **2012**, *37*, 487–513.

40. Yin, Y.; Hong, G.; Xin, B. Preparation and Characterization of Gadolinium Hydroxide Single-Crystalline Nanorods by A Hydrothermal Process. *Chin. Chem. Lett.* **2007**, *18*, 491–494.
41. Hu, C.; Liu, H.; Dong, W.; Zhang, Y.; Bao, G.; Lao, C.; Wang, Z. L. $La(OH)_3$ and La_2O_3 Nanobelts—Synthesis and Physical Properties. *Adv. Mater.* **2007**, *19*, 470–474.
42. Wang, X.; Li, Y. Synthesis and Characterization of Lanthanide Hydroxide Single-Crystal Nanowires. *Angew. Chem., Int. Ed.* **2002**, *41*, 4790–4793.
43. Xiao, X.; Huang, Y.; Dong, F. Synthesis and Application of One-Dimensional $La(OH)_3$ Nanostructures: An Overview. *J. Chem.* **2014**, *2014* (305986), 1–9.
44. Fang, B.; Zhang, W.; Wang, G.; Liu, H.; Wei, S. Microwave-Assisted Preparation of A Carbon Nanotube/$La(OH)_3$ Nanocomposite, and Its Application to Electrochemical Determination of Adenine and Guanine. *Microchim. Acta* **2008**, *162*, 175–180.
45. Mu, Q.; Chen, T.; Wang, Y. Synthesis, Characterization and Photoluminescence of Lanthanum Hydroxide Nanorods by A Simple Route at Room Temperature. *Nanotechnology* **2009**, *20*, 345602.
46. Dixit, S. G.; Vanjara, A. K.; Nagarkar, J.; Nikoorazm, M.; Desai, T. Co-Adsorption of Quaternary Ammonium Compounds—Nonionic Surfactants on Solid−Liquid Interface. *Colloids Surf., A* **2002**, *205*, 39–46.
47. Tang, B.; Ge, J.; Wu, C.; Zhuo, L.; Niu, J.; Chen, Z.; Shi, Z.; Dong, Y. Sol−Solvothermal Synthesis and Microwave Evolution of $La(OH)_3$ Nanorods to La_2O_3 Nanorods. *Nanotechnology* **2004**, *15*, 1273–1276.
48. Wang, W.; Li, Z.; Xu, X.; Dong, B.; Zhang, H.; Wang, Z.; Wang, C.; Baughman, R. H.; Fang, S. Au-Doped Polyacrylonitrile-Polyaniline Core-Shell Electrospun Nanofibers Having High Field-Effect Mobilities. *Small* **2011**, *7*, 597–600.
49. Li, S.; Hu, S.; Du, N.; Fan, J.; Xu, L.; Xu, J. Low-Temperature Chemical Solution Synthesis of Dendrite-Like $La(OH)_3$ Nanostructures and Their Thermal Conversion to La_2O_3 Nanostructures. *Rare Met.* **2015**, *34*, 395–399.
50. Huang, W.; Zhu, Y.; Tang, J.; Yu, X.; Wang, X.; Li, D.; Zhang, Y. Lanthanum-Doped Ordered Mesoporous Hollow Silica Spheres as Novel Adsorbents for Efficient Phosphate Removal. *J. Mater. Chem. A* **2014**, *2*, 8839–8849.
51. Huang, W.; Li, D.; Liu, Z.; Tao, Q.; Zhu, Y.; Yang, J.; Zhang, Y. Kinetics, Isotherm, Thermodynamic, and Adsorption Mechanism Studies of $La(OH)_3$-Modified Exfoliated Vermiculites as Highly Efficient Phosphate Adsorbents. *Chem. Eng. J.* **2014**, *236*, 191–201.
52. Lu, J.; Liu, H.; Zhao, X.; Jefferson, W.; Cheng, F.; Qu, J. Phosphate Removal from Water Using Freshly Formed Fe−Mn Binary Oxide: Adsorption Behaviors and Mechanisms. *Colloids Surf., A* **2014**, *455*, 11–18.
53. Febrianto, J.; Kosasih, A. N.; Sunarso, J.; Ju, Y.; Indraswati, N.; Ismadji, S. Equilibrium and Kinetic Studies in Adsorption of Heavy Metals Using Biosorbent: A Summary of Recent Studies. *J. Hazard. Mater.* **2009**, *162*, 616–645.
54. Hameed, B. H.; Ahmad, A. A.; Aziz, N. Isotherms, Kinetics and Thermodynamics of Acid Dye Adsorption on Activated Palm Ash. *Chem. Eng. J.* **2007**, *133*, 195–203.
55. Zong, E.; Wei, D.; Wan, H.; Zheng, S.; Xu, Z.; Zhu, D. Adsorptive Removal of Phosphate Ions from Aqueous Solution Using Zirconia-Functionalized Graphite Oxide. *Chem. Eng. J.* **2013**, *221*, 193–203.
56. Mu, Q.; Wang, Y. Synthesis, Characterization, Shape-Preserved Transformation, and Optical Properties of $La(OH)_3$, $La_2O_2CO_3$, and La_2O_3 Nanorods. *J. Alloys Compd.* **2011**, *509*, 396–401.
57. Liu, J.; Zhou, Q.; Chen, J.; Zhang, L.; Chang, N. Phosphate Adsorption on Hydroxyl−Iron−Lanthanum Doped Activated Carbon Fiber. *Chem. Eng. J.* **2013**, *215−216*, 859–867.
58. Zhang, L.; Zhou, Q.; Liu, J.; Chang, N.; Wan, L.; Chen, J. Phosphate Adsorption on Lanthanum Hydroxide-Doped Activated Carbon Fiber. *Chem. Eng. J.* **2012**, *185−186*, 160–167.
59. Xie, J.; Wang, Z.; Fang, D.; Li, C.; Wu, D. Green Synthesis of A Novel Hybrid Sorbent of Zeolite/Lanthanum Hydroxide and Its Application in The Removal and Recovery of Phosphate from Water. *J. Colloid Interface Sci.* **2014**, *423*, 13–19.
60. Zhao, D.; Sengupta, A. K. Ultimate Removal of Phosphate from Wastewater Using A New Class of Polymeric Ion Exchangers. *Water Res.* **1998**, *32*, 1613–1625.
61. Li, C.; Ma, J.; Shen, J.; Wang, P. Removal of Phosphate from Secondary Effluent with Fe^{2+} Enhanced by H_2O_2 at Nature Ph/Neutral Ph. *J. Hazard. Mater.* **2009**, *166*, 891–896.
62. Kim, S. L.; Paul Chen, J.; Ting, Y. P. Study on Feed Pretreatment for Membrane Filtration of Secondary Effluent. *Sep. Purif. Technol.* **2002**, *29*, 171–179.
63. Kang, S. K.; Choo, K. H.; Lim, K. H. Use of Iron Oxide Particles as Adsorbents to Enhance Phosphorus Removal from Secondary Wastewater Effluent. *Sep. Sci. Technol.* **2003**, *38*, 3853–3874.
64. Gibbs, M. M.; Hickey, C. W.; Özkundakci, D. Sustainability Assessment and Comparison of Efficacy of Four P-Inactivation Agents for Managing Internal Phosphorus Loads in Lakes: Sediment Incubations. *Hydrobiologia* **2011**, *658*, 253–275.
65. Li, H.; Ru, J.; Yin, W.; Liu, X.; Wang, J.; Zhang, W. Removal of Phosphate from Polluted Water by Lanthanum Doped Vesuvianite. *J. Hazard. Mater.* **2009**, *168*, 326–330.